

THE GEOPHYSICAL INVESTIGATION OF BANTEN GEOTHERMAL AREA , WEST JAVA

Mulyadi

GEOTHERMAL DIVISION , EXPLORATION AND PRODUCTION , PERTAMINA

ABSTRACT

Most of the geophysical techniques that usually form part of Indonesian geothermal prospecting program have been used to explore the Banten geothermal area, West Java. A composite interpretation of Bouguer gravity, DC Resistivity, Magnetotelluric and Passive seismic surveys has indicated the presence of two geothermal prospects in the Banten area. The more obvious geothermal prospect is located on the southern slope of G. Karang, in the vicinity of the village of Mengger, while the less well defined Mendong prospect is associated with hydrothermal springs SW of G. Karang.

A deep exploratory well, Bn-1, is currently being drilled in the Mengger area in order to test the composite interpretation of the exploration surveys.

INTRODUCTION

The Banten geothermal prospect area is located 50 km west of Jakarta, (Figure 1). Surface thermal manifestations which include numerous hot springs and solfataric vents lying on the slope of G. Karang and at the summit of G. Pulosari first attracted interest to this area.

Geological, geophysical and geochemical surveys have been conducted over the Banten area by Pertamina and several companies since 1975. Schlumberger resistivity soundings were carried out by Kyushu Electric Power Co., Inc. (Japan) in 1975 followed by a more detailed program in 1977. Geological and magnetotelluric surveys were conducted in 1977 to 1979 with the assistance of BEICIP (France). In 1983, Pertamina contracted GEOCO (CGG, France) to complete an additional magnetotelluric survey in order to delineate deeper resistivity structure. A passive seismic survey and additional geophysical and geological programs recently been completed by Pertamina.

Geological Framework

The Banten geothermal area is located in west Java adjacent to two Pliocene - Pleistocene andesitic stratovolcanoes, G. Pulosari and G. Karang. The regional basement consists of granodiorite intrusive

rocks overlain by the Bojongmanik Formation, a sequence of marine Tertiary sediments interlayered with pyroclastic volcanic rocks. The sediments outcrop in the southern part of the prospect area but their thickness is unknown. A tentative lithostratigraphic column is suggested in Table 1.

A geologic interpretation of aerial photographs (EEICIP - PERTAMINA) showed that the large families of faults illustrated in Figure 2 have mainly NW-SE strike in the prospect area and continue into South Sumatra. The Citaman hot springs and the Cibiuk warm springs south of G. Karang are closely related to these structures and are important in defining the Mengger and Mendong prospects. A system of NESW faults to the north of G. Karang are associated with hydrothermal springs NW of G. Karang (Delarue, 1979). Although these springs might be indicative of a geothermal prospect, they will not be discussed in this paper.

GEOPHYSICSTemperature Gradient

The results from fifteen temperature gradient holes drilled in the Banten area, ranging from 100 m to 150 m depth, are illustrated in figure 3. The first location, hole 1, drilled near the Citaman hot springs was influenced by flow from the shallow hydrothermal system since the temperature increased suddenly to 55°C at 15 m depth from the mean air temperature of 22°C and then remained constant down to a total depth of about 100 m. In general, the temperature gradient of 4.4°C/10 m in the northern part of the area decreases towards the south to 1.1°C/10 m. The gradient of 1.93°C/10 m which was observed in hole 7 is unusual, since the gradient in hole 9, about 1 km away from hole 7, was 4.4°C/10 m. This implies that hole 7 was not deep enough to give useful temperature gradient data.

Resistivity

The lateral distribution of shallow resistivity from Schlumberger profiling at AB/2 = 500 m and 1000 m can be seen in Figure 4. The contour only delineates the

north and the west boundary of the shallow conductive area. The re-interpreted BETCIP MT data are presented as longitudinal conductances (Kaufman and Keller, 1981) in Figure 5a, while the structure of the maximum depth of the conductive layer is illustrated in Figure 5b. The northern conductive zone which has conductances greater than 300 mho has maximum depth of about 600 m below sea level. The eastern, 300 - 500 mho conductive zone appears at an elevation of about 200 to 400 m below sea level and underlies the Citaman hot springs. The southern, greater than 300 mho conductance anomaly appears at elevation varying from 300 m to 500 m below sea level. The more recent MT survey which was conducted by GECO shows a resistivity pattern at skin depths of 500 m and 3000 m similar to the conductance map produced using the EEICIP data (Mulyadi, Pertamina report in preparation).

Gravity

About 220 gravity station observed in 1984 were included in the Banten Bouguer map. A reduction density of $2.67 \times 10^3 \text{ kg/m}^3$ was used for the Bouguer and terrain correction (Hammer zones A to I) computations. This is probably slightly high since andesitic lavas which are exposed in the Banten area and similar rocks encountered in other Indonesian areas have a density of about $2.85 \times 10^3 \text{ kg/m}^3$ (Sudarman and Hochstein, 1983). A simple regional trend obtained from trend surface analysis order one was removed resulting in the residual map in Figure 6. Positive residual anomalies appear at Mengger (+ 6 mgal) and Medong (+ 4 mgal), and three negative residual anomalies (- 4 mgal) appear in the north, in the south, in the south west, and in the north-east part of the area.

Micro Earthquake

A WSSN earthquake catalogue for Java has been maintained by the Badan Meteorologi dan Geofisika, Indonesia, for geological purposes. However, the data available during 1949 - 1963 had few magnitude and depth determinations. Fortunately, the data available during the period of 1963 - 1982 were of better quality (PT. Geoservices report for Pertamina, 1985), and the magnitude (analogous to Richter magnitude) over 4 and depth of those earthquakes have been plotted in Figure 7. It seems that no earthquakes greater than magnitude 4 (the nominal WSSN threshold) had occurred over the Banten geothermal area during this period.

Because Pertamina has recently been investigating the use of passive seismic monitoring in geothermal exploration with some success, it was decided to install a microearthquake detection system at Banten. Four Sprengnether MEQ-800 smoked drum microearth-

quake recorders using L4C seismometers were deployed as in Figure 8 for period of four months in 1985. Unfortunately, recorder number 2 was stolen early in the survey so that only three stations produced usable data. A drum speed of 60 mm/minute was used and the units were time synchronized by correlating the MEQ-600 clocks with an external TS-400 clock every 24 hours.

The radial distance to micro earthquake event was estimated from the P and S arrival picks using the following equation :

$$D = (T_p - T_s) \cdot V_p \cdot V_s / (V_p - V_s)$$

where :

D is the distance of event estimated from recorder,

V_p is the velocity of compressional wave (km/s),

V_s is the velocity of shear wave (km/s),

T_p is the arrival time of compressional wave, and

T_s is the arrival time of shear wave.

The ratio $V_p \cdot V_s / (V_p - V_s)$ was approximated as 7.5 km/s based on measurements of andesites sampled in the Dieng geothermal area at 10 m to 30 m depth (Summarized in Table 2).

The microearthquake hypocenters were determined geometrically using the radial distances calculated for each station.

The high value for $V_p \cdot V_s / (V_p - V_s)$ compared to 4.4 km/s modelled at the Geysers (Eberhart - Phillips and Oppenheimer, 1984) and 7.0 km/s in a volcanic area of Papua - New Guinea (Carmichael, R., 1982) is consistent with the low Poisson's Ratio observed in other geothermal areas in Java (Mulyadi and Nugroho, in prep. 1985).

Of 261 earthquakes recorded during the survey, sufficient data was gathered to analyse and locate 108 events. The following discussion will use the depth of these located earthquakes to define prospective areas in a manner similar to that used at Grass Valley, Nevada by Majer (1978) and at the Geysers by Majer and McEvilly (1979). But no other earthquake parameters will be presented at this time.

DISCUSSION

Majer (1978) found that the depths of micro earthquakes beneath Grass Valley, Nevada are within the range 0 - 8 km, contrasting with the typical 10 - 15 km for the region. Majer and McEvilly (1979) noted that the maximum earthquake depth was about 5 km beneath the Geysers as compared to 11 - 12 km for the surrounding region. Using a more complete data set, Eberhart - Phillips and Oppenheimer (1985) have interpreted the shallow Geysers microearthquake activity as being likely associated with volumetric contraction due to mass withdrawal during production of the steam field. A seismic survey at the Kamojang geothermal field

similar to the Banten micro earthquake survey indicated that the average earthquake depth was about 4 km over the production zone and over two positive residual gravity anomalies outside the field which are considered prospective, while depths over 6 km occur in the surrounding areas (Mulyadi and Nugroho, in preparation, 1985). Extending this technique to the Banten area should aid in the delineation of the geothermal prospect. The average depth of Banten region microearthquake of about 6 to 7 km was subtracted from the depth determinations and these values were plotted at the epicenter locations. The residual microearthquake depth map (Figure 8) thus had produced a positive (+ 2 km) residual anomaly which coincided with the geological structures and anomalous thermal gradient in the north east of Mengger.

The lateral distribution of the shallow conductive layer which is defined by the 10 ohm-m Schlumberger resistivity contour may correspond to elevated temperature since the anomalous temperature gradients are within the conductive area (Figure 3 and 4). Layered models of GEOCO MT data indicate the conductive layer varies with a thickness of about 500 m and resistivity of 1.5 - 3.0 ohm-m in the north compared to a thickness of 500 - 750 m and resistivity of 2 ohm-m in the south near Kedong. The low resistivities at Medong are associated with thick Tertiary sediments and Quaternary volcanic products. These rocks may overlie the resistive andesitic intrusion indicated by the small gravity anomaly at Medong. The high resistivity half space below the conductive layer in the Mengger area may be a basaltic sill with a density of about $3.03 \times 10^3 \text{ kg/m}^3$ (Armstrong, 1984). It apparently originated from G. Pulosari, and forms an elliptical residual gravity anomaly with axes of about 5 km and 7 km (Figure 6). It is associated with the deep microearthquake hypocenter anomaly surrounding the village of Mengger. A cylindrical slab of density $3.03 \times 10^3 \text{ kg/m}^3$ would produce a 3.5 km half wave length anomaly of +8 mgal in country rock of density $2.67 \times 10^3 \text{ kg/m}^3$ with a top at about 1.36 km depth and a radius of about 1.36 (Parasnis, 1969). The surface resistivity layer made of unlabeled lahars, breccias andesite and pyroclastic flows.

The occurrence of resistive substratum within the prospect area often indicates where the reservoir is present. If this is the case, the Tertiary marine sediments of the Bojongmanik Formation with high rank alteration may act as the reservoir. This is also supported by the high boron concentration in the hot springs illustrated in Table 3. The high boron concentrations originate from water that has interacted with marine sediments and has subsequently boiled, allowing high temperature steam to carry the boron to the ground surface (Tonani and Bencini, 1979).

A high temperature system in this area would be associated with the recent volcanism of G. Karang and G. Pulosari. The interpreted outflow of the geothermal fluids to the south of G. Karang is supported by the shallow (+ 2 km) microearthquake hypocenters.

A total depth of 2000 m is being suggested for the first well in the Mengger prospect area. The Na/K and Na/K/Ca geothermometers indicate high (260°C) reservoir temperatures. Using a linear gradient from holes 7 and 9, temperature was extrapolated to 100°C and assuming boiling at this depth, the temperature was further extrapolated along the boiling point curve to 260°C which occurs at a depth of about 900 - 1000 m (Sudarman, Pertamina internal report, 1985). Therefore, it is expected that the reservoir may be encountered at this depth in En-1.

The other positive Bouguer residual anomaly which appeared at the southern area around Keaong is possibly due to a shallow dense body. The temperature gradient anomaly of $2^\circ\text{C}/10 \text{ m}$ near Medong suggests that the dense body may be an andesitic intrusion which supplies high temperature to the surrounding area and forms the source of the 32°C warm springs with H_2S and CO_2 emission.

Delarue's 1975 interpretation that the system is associated with north west - south east faults through G. Karaiig is considered unlikely. The MT data at Medong do not help much in defining the geothermal system because the relatively thick, conductive sandy marl layers which cap the resistive substratum cause a current accumulation at shallow depths, thus limiting the depth of investigation.

CONCLUSIONS AND SUGGESTIONS

The geophysical and geological investigations illustrated in the composite map in Figure 9 indicate that the Mengger and Medong prospects should be drilled in order to obtain adequate sub-surface information. The Mengger prospects is currently being tested with well En-1. The second prospect, Medong, is only marked by a positive Bouguer anomaly and warm springs. Although the temperature gradients over this area are relatively high, they may be outflow from G. Karang. Therefore, it is regarded as a lower priority target.

To remove some of the uncertainty about the Medong area, it may be useful to conduct a passive seismic survey. This technique has successfully indicated the boundary of the production zone at the Kamojang field and MT surveys have failed to probe deep enough in the area which is covered by a very thick conductive layer.

ACKNOWLEDGEMENT

The author would like to acknowledge Pertamina Management for permission to publish this paper.

Location	Height m	Temp °C	pH	Q lpm	20°C	Concentration in eq./l. except SiO ₂ & H ₂ BO ₃													
						Ca	Mg	Na	K	CO ₃	SO ₄	Cl	SiO ₂	F	H ₂ BO ₃	Li	Fe	HH ₄	
						(meq/l.)					(mol/l.)								
Cold springs:																			
Kecapi (cr1)	150	232	250	8.4	774	124	785	135	344	105	736	224	56	236	147	-	26		
Citaman (cr2)	185	285	40	7.9	114	685	189	806	214	145	708	164	56	23	67	-	26		
Citaman (cr4)	185	29	200	8.3	124	765	545	885	244	185	936	194	57	15	68	-	26		
River waters:																			
Citaman (ar1)	190	32	-	8.2	114	655	705	125	221	185	155	174	56	25	67	-	-		Travertine deposits
Cibuk (m1)	70	28	-	5	535	445	635	916	124	185	135	705	507	25	67	-	-		
G Karang (n1)	900	20	1500	7.9	505	335	255	686	104	145	156	124	106	25	68	-	26		
Hot springs:																			
Citaman (cr1)	160	45.5	5	8.6	135	244	764	134	764	144	304	234	56	255	236	66	26		Iron hydroxide and
Citaman (cr2)	190	67	2500	9	365	264	834	154	834	164	324	724	807	285	296	66	26		silica travertine d.p.
Cibuk (cr1)	70	31	10.2	114	295	133	145	204	224	114	104	115	0.5	106	-	-	-		CO ₂ & H ₂ S gases
Cibuk (cr1)	70	38	10	8.5	775	815	434	835	624	814	804	535	536	526	-	-	-		with pyrite.
Salt lakes:																			
G Karang	1250	84	92	10	17	504	334	231	205	19	102	2664	34	845	234	527	163534		CO ₂ , H ₂ S, H ₂ O, and SO ₄ (?)
(ar1/2)																			Sulphur deposit and altered rocks without pyrite.

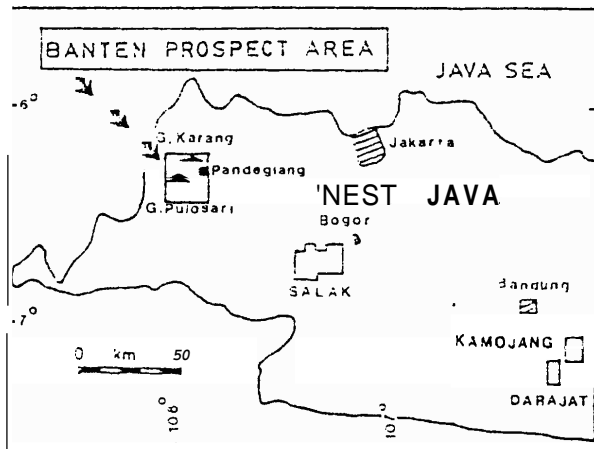


Figure 1 : Location of the Banten Geothermal Prospect .

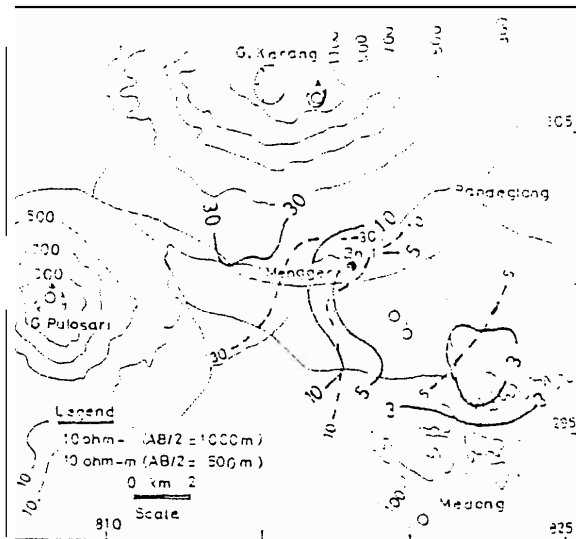


Fig.4. : Map showing the apprent resistivity (Shlumberger) contour.

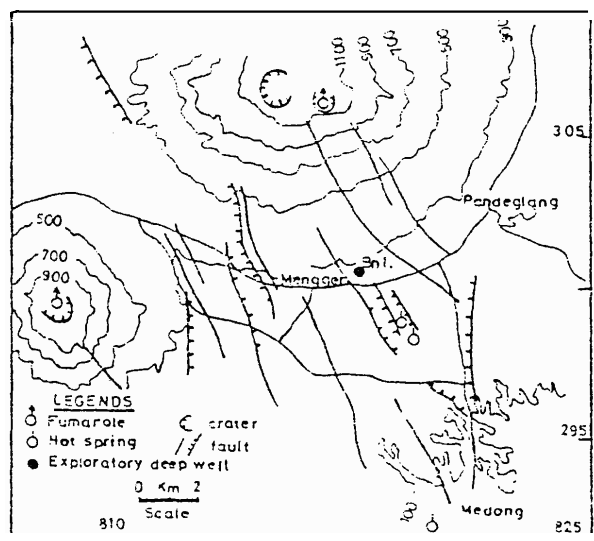


Figure 2: Banten geologic structures and thermal manifestations .

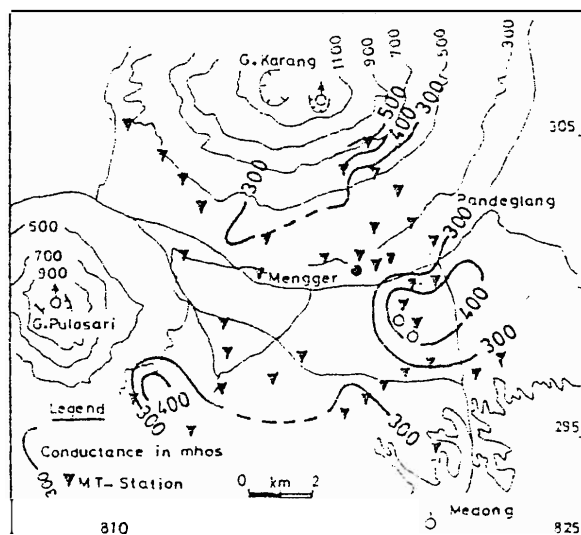


Fig.5a.: MT-Longitudinal Conductance at the Banten prospect .

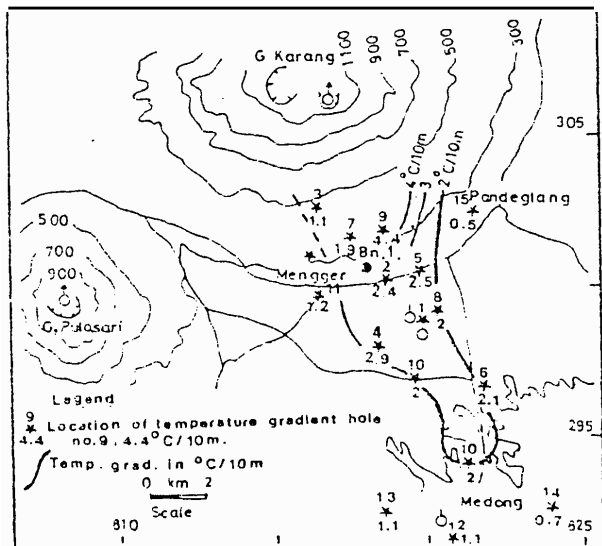


Fig.3. : Temperature gradients at the Banten prospect .

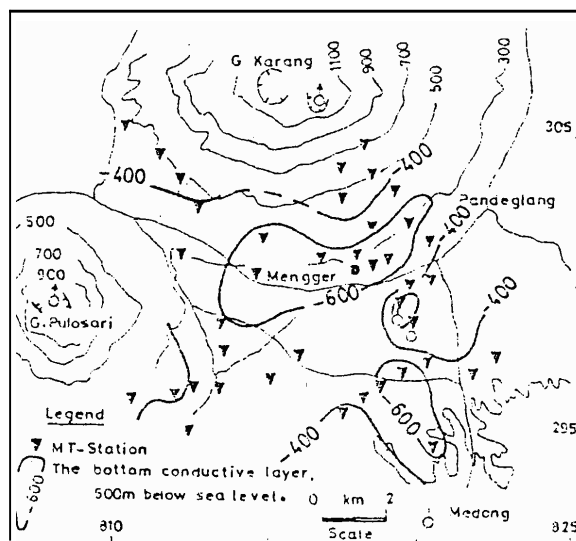


Fig.5b. : Depth to the bottom of the con-
ductive layer from MT at Banten.

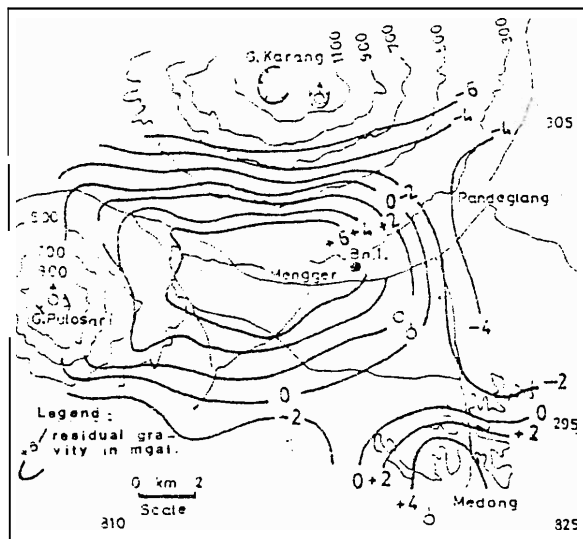


Fig.5.: The residual gravity map of Banten prospect.

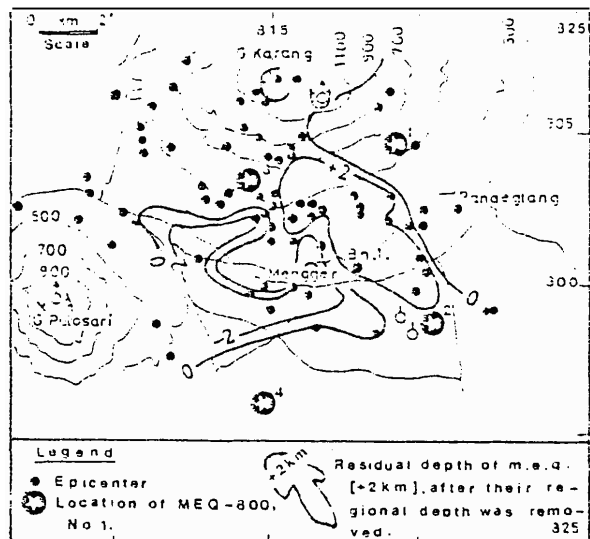


Fig.8.: The residual depth of microearthquake at Banten prospect.

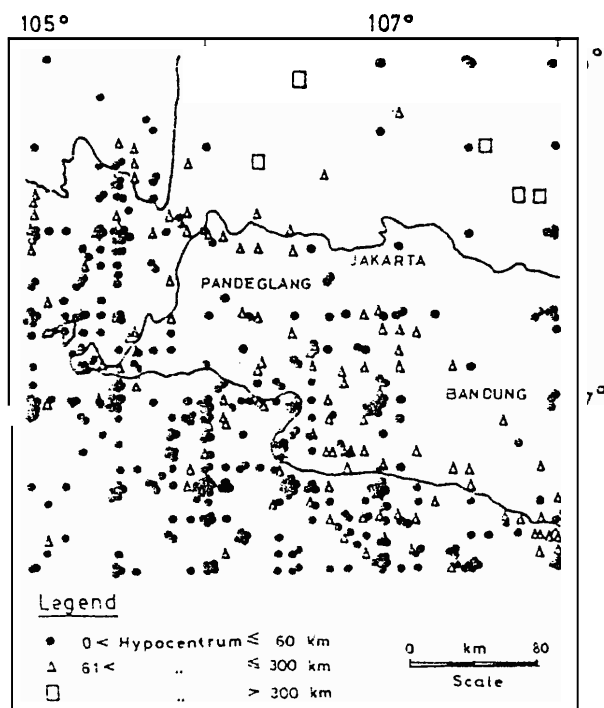


Fig.6.: The epicentrum map with magnitude over 4R of Banten prospect

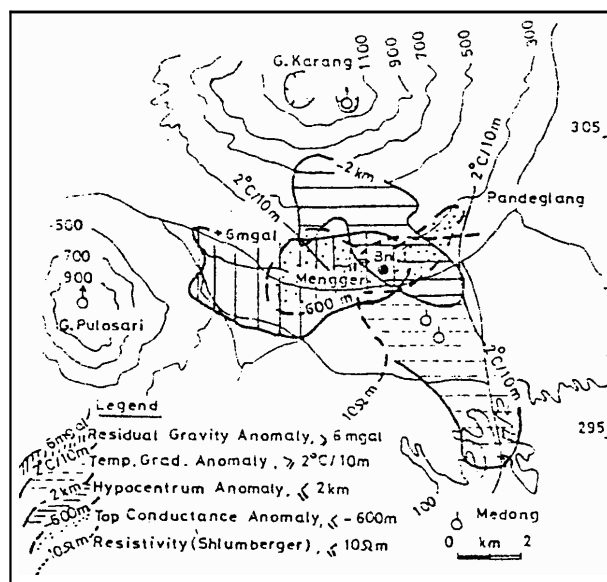


Fig.9 : The geophysical anomaly map of Banten prospect